The effect of Pr substitution on the spectrum and photocatalytic performance of MgAl$_2$O$_4$ nanoparticles

Z. J. Yu [a], J. B. Zhou [a], M. H. Xu [a,*], Y. F. Yang [a], Y. Y. Wang [b]

[a] *Department of Materials Engineering, Huzhou University, Huzhou 313000, P. R. China*

[b] *Huzhou Key Laboratory of Green Energy Materials and Battery Cascade Utilization, Huzhou College, Huzhou, Zhejiang, 313000, P. R. China*

To study the spectral regulation of Pr on MgAl$_2$O$_4$ nanoparticles, different contents of Pr doped MgAlPr ternary hydrotalcite were synthesized by co-precipitation method, and Pr containing mixed metal oxides Pr-*x-y* was prepared by high-temperature calcination. The Pr had little effect on the morphology of hydrotalcite, but significantly improved the heat resistance. The Pr significantly reduced the Eg values of MgAl-L and its mixed oxide (Eg=1.68–1.87 eV). After 100 min of irradiation with visible light, the degradation rate of MB reached 87.7%. In the reaction system of Pr-0.05-500/H$_2$O$_2$, *h*+ played a major role. There was a corresponding relationship between the photocatalytic performance and *L** value of mixed oxide nanoparticles based on MgAl-L and Pr-0.05-L. The NIR of hydrotalcite or Pr containing nanoparticles was greatly affected by the calcination temperature and Pr containing, but the values of NIR were more than 50%.

1. Introduction

Hydrotalcite-like compounds are a type of layered double hydroxides (LDHs), which contains positively charged layers and negatively charged anions between layers [1, 2]. Because of the different choices of layered metals and interlayer anions in hydrotalcite, LDHs have different compositions [3, 4]. Thus, hydrotalcite exhibits excellent catalytic performance [5-7]. On the other hand, mixed metal oxide nanoparticles can be obtained by adjusting the types and quantities of metal ions in LDHs laminates and calcining them at high temperatures [8, 9].

In addition, LDHs materials can form excellent active mixed metal oxides (MMO) that have thermal stability and high specific surface area when calcined at moderate temperatures (300–600 ºC) [10]. Especially, MMO prepared by LDHs heat treatment can regulate the semiconductor properties and promote the movement of photo generated electrons on the surface of photocatalysts, which can be used as photocatalysts for degrading organic pollutants [11]. Due to the diversity of LDHs chemical composition, the preparation of MMO based on hydrotalcite has always been a focus of attention. R Trujillano *et al.* investigated the adsorption and photocatalytic degradation of 4-Nitrophenol by ZnAl-L and its mixed oxide attained after calcination at 650 ºC [5]. They found that the adsorption and degradation effect of calcined hydrotalcite is better. *Po Hsiang Chang et al.* investigated the removal performance of perfluorinated compounds by calcined hydrotalcite (CHT) based on perfluorooctane sulfonate. The CHT could be regenerated when PFOS-saturated HT was calcined at 450 ºC for 3 h, and the ability to remove full PFOS also recovers [12]. T Turk *et al.* studied the removal effect of arsenic from water with calcined Fe-hydrotalcite (CFeHT), which was LDHs prepared through co-precipitation method [13]. Chen *et al.* reported that combine MoS$_2$ with hydrotalcite to degrade methylene blue, its degradation rate can reach 93 % after 30 min of adsorption and 150 min of illumination [14]. The photocatalytic effect is higher, but the illumination

time is also longer. More importantly, introducing alkaline rare earth elements such as La, Y or Ce into these materials can alter the alkaline sites of oxides, thereby regulating the basicity of catalysts [15].

The rapid valence state transformation of rare earth elements endows rare earth oxides with characteristics such as cationic valence state, lattice oxygen transfer, paramagnetic behavior and alkaline surface [16]. It is worth noting that these characteristics are inherently related to the activity of many catalysts. Based on the characteristics of rare earth elements, introducing rare earth elements into LDHs is expected to prepare precursors with high catalytic activity. Ternary layered double hydroxides precursors such as ternary mixed metal oxides (MgAlLa-M), lamellar photocatalyst In_2S_3/g-C_3N_4/CoZnAl-LDH, NiFeCo LDH vertical nanosheet arrays (NiFeCo-LDH-NA), molybdenum and vanadium modified catalysts such as V/Mg-Al and Mo/Mg-Al, Mg/Al/Zr hydrotalcite-like compounds catalysts were reported [17-19]. But, few reports on praseodymium-containing mixed oxide derived from ternary LDHs, especially lacking in research on the regulation of visible and near-infrared spectra of composite oxides by Pr.

Therefore, from the perspective of resources and practical applications, introducing rare earth metal elements into oxides to prepare high-performance catalysts is beneficial for expanding the application of metal elements [20, 21]. Recently, it is worth noting that the research and development of materials with high near-infrared reflectance (NIR) have attracted widespread attention [22, 23]. Near infrared reflective materials, especially pigments, can reflect the near-infrared energy in the sunlight on the surface of the covering material, thereby reducing the use of refrigeration equipment, saving electricity, and reducing carbon emissions [24].

In order to efficiently utilize the exchange performance of metal cations on the hydrotalcite layer [25], and excavate the high photocatalytic activity of rare earth elements, a series of mixed oxide nanoparticles based on MgAlPr hydrotalcite (Pr-x-L (x=0.025, 0.05, 0.1 and 0.2)) with different Mg/Al/Pr ratios were synthesized through co-precipitation method. In addition, the photocatalytic effect was evaluated with measuring the degradation of MB under 150 W halogen lamp irradiation. In addition, the possible mechanisms of photodegradation were also proposed. At the same time, the color of the CIE coordinate and near-infrared reflectance performance of hydrotalcite based mixed oxide were further studied. The research with photocatalytic and near-infrared reflectance properties of mixed metal oxides containing Pr is expected to develop a material that combines photocatalytic activity and can reflect solar energy, which can be applied in specific occasions.

2. Experimental section

2.1. Materials

$Mg(NO_3)_2 \cdot 6H_2O$, $Pr(NO_3)_3 \cdot 6H_2O$, $Al(NO_3)_3 \cdot 9H_2O$, Na_2CO_3, NaOH, isopropanol, EDTA-Na, p-benzoquinone, H_2O_2 and methylene blue (MB) were analytical purity, and provided by Aladdin reagent (Shanghai) Co., Ltd.

2.2. Synthesis of mixed oxide

The MgAlPr-LDHs with different molar ratios of Al(III)/Pr(III) were synthesized according to literature [16]. According to molar ratio of M(II)/M(II) was 3.0. Certain quality of $Mg(NO_3)_2 \cdot 6H_2O$, $Pr(NO_3)_3 \cdot 9H_2O$ and $Al(NO_3)_3 \cdot 6H_2O$ solid were dissolved, the above solution was solution A. Solution B was a mixed solution of Na_2CO_3 and NaOH dissolved. Under stirring, slowly drop the above two solutions into a beaker containing a small amount of distilled water. During the stirring process, to adjust the pH value to 9~10 using NaOH solution. After dropping, continue stirring the above solution for 0.5 h. After that, the obtained slurry was placed in a 65 °C oven for 24 h. Collecting sediment through centrifugal separation and then washing multiple times with distilled water. Finally, the solid was dried at 70 °C to get MgAlPr-LDHs precursors with different Mg/Al/Pr molar ratios (*i.e.*, 3:0.975:0.025, 3:0.95:0.05, 3:0.9:0.1, 3:0.8:0.2), these precursors were labeled as Pr-x-L, the x was the molar ratio of Pr(III). When the Mg/Al/Pr molar ratio was 3:1:0, the sample was labeled as MgAl-L, the one with Mg/Al/Pr molar ratio of 3:0.975:0.025 was labeled as

Pr-0.025-L. The samples of other proportions are marked as Pr-*x*-L (*x*=0.025, 0.05, 0.1 and 0.2).

Calcine the prepared hydrotalcite precursor in air for 4 h at a calcination temperature range of 400 to 600 °C. When the samples obtained from calcination at 400 °C were labeled as MgAl-LDO-400. The mixed oxide with different Pr contents obtained by calcination at different temperatures were labeled as Pr-*x*-y, (*x*=0.025, 0.05, 0.1 and 0.2, *y* represents the calcination temperature, *y*=400, 500 and 600). Pr-0.025-400 represents the mixed oxide obtained by calcining Pr-0.025-L at 400 °C. The labeling methods for samples at other temperatures and Pr content were similar.

2.3. Characterizations

The morphology of Pr-*x*-y was observed by SEM (S-3400N, Hitachi, Japan). The crystal structure of Pr-*x*-y was identified by X-ray diffractometer (Beijing Purkinje General Instrument Co., Ltd., China), the testing conditions are as follows: Cu Kα, λ=0.1545 nm, pipe current 20 mA, pipe voltage 36 kV. UV−Vis diffused reflectance spectra (DRS) of the prepared samples were tested by a UV-Vis spectro photometer (ISA-220, Thermo, USA).

2.4. Photocatalysis

The photocatalytic experiments were conducted based on references [16]. The photocatalytic activity were assessed through photodegradation of MB solution under visible light irradiation for 0.5 h (150 W halogen lamp). Added photocatalyst (0.05 g) to 25 mL MB (5 mg/L) aqueous solution, sonicate for 2 min, and then added H_2O_2 (30% *w/w*, 0.5 mL). For the light experiment, catalyst was added into MB solution and was vigorously stirred without light for 0.5 h to ensure adsorption and desorption equilibrium was reached. After that, photocatalytic degradation was carried out under visible light irradiation of a 150 w halogen lamp. Every 20 min, the solution sample used for analysis was extracted and immediately centrifuged. Afterwards, the absorbance value of the filtrate at 664 nm was measured with UV-Vis spectroscopy (752). The effects of calcination temperature and the content of Pr on the degradation of MB were studied.

2.5. Color and UV-Vis-NIR measurements

Based on visible light reflection spectra and combined with color CIE software, the CIE Lab color data (*L**, *a** and *b**) were calculated with spectrum range was 400-700 nm (CIE D65 as photo source, and observation angle was 10 °, Perkin-Elmer) [26]. Usually, *L** is the lightness axis (*L** value greater than 0 indicates white, otherwise it indicates black). If the value of *a** is greater than 0, it indicates red, if the value of *a** is less than 0, the color will appear green. The *b** value greater than 0 indicates yellow, otherwise it indicates blue. The parameters *a** and *b** indicate the hue or color of the pigments [24].

2.6. UV-Vis-NIR measurements

The Near-infrared reflectance (R), which is between 700 nm and 2500 nm can be calculated using the following formula:

$$R = \frac{\int_{700}^{2500} r(\lambda)i(\lambda)d\lambda}{\int_{700}^{2500} i(\lambda)d\lambda} \tag{1}$$

where $r(\lambda)$ (W·m^{-2}) represents the reflectance of spectral got from the UV–Vis–NIR spectrophotometer, and $i(\lambda)$ (W·m^{-2}·nm^{-1}) represents the solar spectral irradiance got based on ASTM standard G159-98 [24, 27]. The value of near-infrared reflectance can be used to quantify solar radiation and study the reflection performance of materials.

3. Results and discussion

3.1. X-ray diffraction

The XRD patterns of MgAl-L precursors at different calcination temperatures (Fig.1a) reveal that the diffraction peaks of MgAl-L at 2θ=11.7 $^\circ$, 22.5 $^\circ$, 34.5 $^\circ$, 60.2 $^\circ$, and 62.4 $^\circ$ can be assigned to (003), (006), (009), (110) and (113) crystal plane of LDHs, respectively, which is consistent with the JCPDS 48-0601 standard card and corresponds to the layered structural characteristics of hydrotalcite [28, 29]. This indicates that the prepared MgAl-L has a unique layered structure of hydrotalcite. Additionally, in 2θ=29.1 $^\circ$, 42.6 $^\circ$ and 62.1 $^\circ$, MgAl-L transformed into mixed oxide under calcination at 400 $^\circ$C, and oxides such as MgO, Al_2O_3, and $MgAl_2O_4$ are found in the jade analysis comparison card. Under calcination at 500 $^\circ$C and 600 $^\circ$C, there are no peaks of MgO. But in 2θ= 42.6 $^\circ$ and 62.1 $^\circ$, MgAl-L generates two main oxides, Al_2O_3, and $MgAl_2O_4$. And the higher the calcination temperature, the sharper the diffraction peak of the produced substance, indicating a higher crystallinity of the substance.
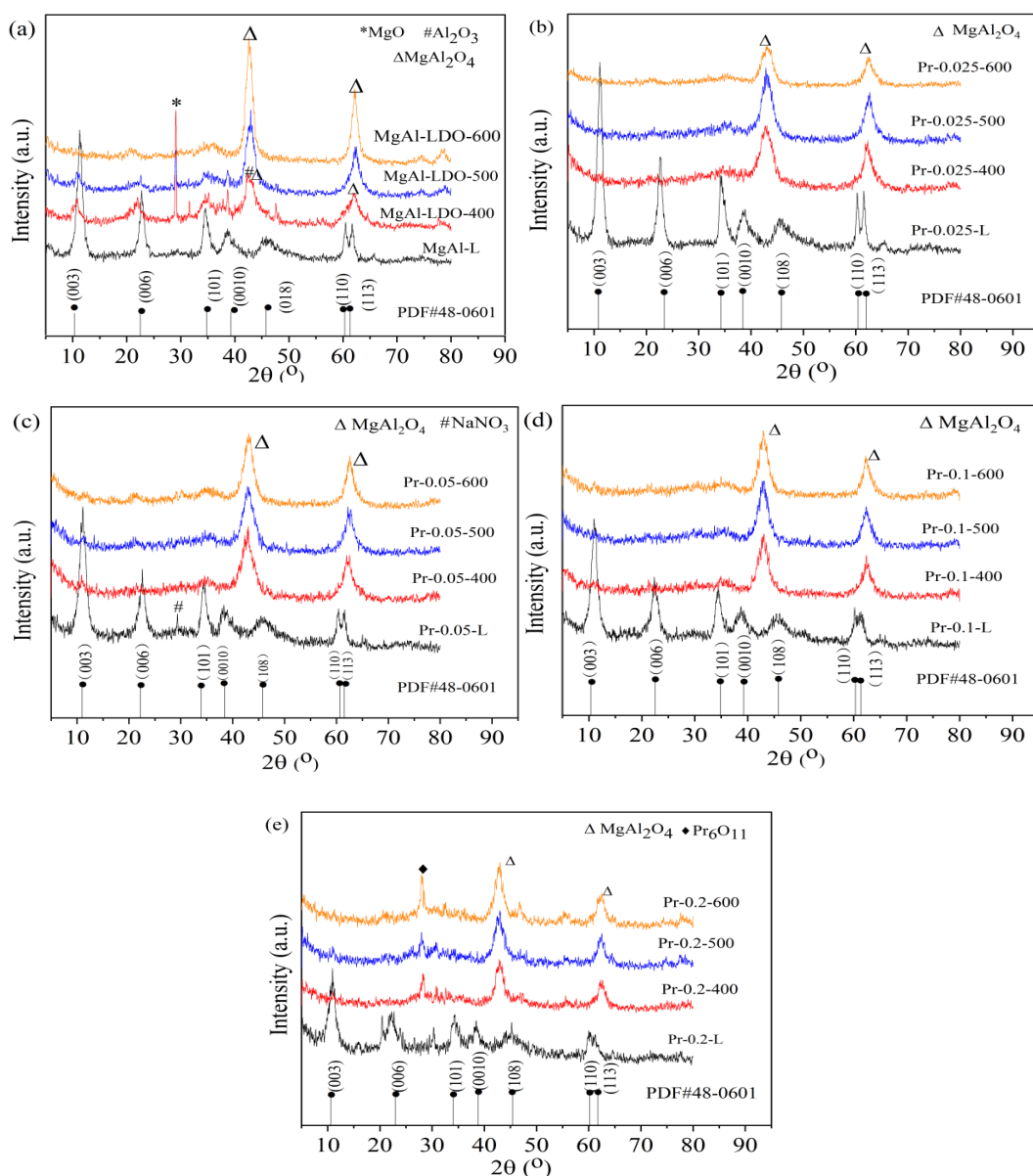

Fig.1. XRD pattern of MgAl-L, Pr-x-L (x: 0.025, 0.05, 0.1 and 0.2) and their mixed oxide.

From the Fig.1b, it can be seen that when Pr replaces some Al to synthesize Pr-0.025-L, its diffraction peak pattern is sharp, with higher intensity and fewer impurity peaks, indicating Pr-0.025-L has a higher crystallinity. The characteristic diffraction peak of hydrotalcite appear, indicating that the substitution of some Al with Pr does not affect the synthesis of hydrotalcite and maintained the interlayer structure of hydrotalcite. However, after calcination at temperatures ranging from 400 to 600 °C, the OH^- and CO_3^{2-} of LDHs are rapidly removed, and the corresponding diffraction peaks of each crystal face of hydrotalcite disappear. At $2\theta= 62.1$ °, a new diffraction peak appears, which is an oxide mainly composed of $MgAl_2O_4$. This indicates that hydrotalcite has been calcined to produce mixed oxide. In addition, there are no oxides of Pr present, and we speculate that Pr maybe still partially replace Al, generating the isomorphic substance $MgPr_2O_4$ of $MgAl_2O_4$.

When increasing the content of Pr to synthesize Pr-0.05-L and Pr-0.1-L (Fig.1c and Fig.1d), their diffraction peak spectra are similar to Pr-0.025-L, indicating that they also have layered structure of hydrotalcite. After calcination at different temperatures, the mixed oxide generated is mainly $MgAl_2O_4$. About Pr-0.2-L, the crystallinity of hydrotalcite decreases, and after calcination at temperatures ranging from 400 to 600, except for $MgAl_2O_4$, an oxide Pr_6O_{11} appears at $2\theta=28.1$. And as the calcination temperature increases, the diffraction peak of Pr_6O_{11} becomes sharper, indicating Pr_6O_{11} has higher crystallinity. This is because too much Pr cannot completely replace Al to form hydrotalcite, which may led to the formation of compounds containing Pr during the reaction process. After calcination, Pr_6O_{11} is formed.

In addition, after the addition of Pr, the diffraction peaks of Pr-0.025-L and Pr-0.05-L on the (003) crystal plane are both at $2\theta=11.1$ °, the diffraction peaks of Pr-0.1-L and Pr-0.2-L (Fig.1e) on the (003) crystal plane are at $2\theta=11$ °. Comparing the diffraction peaks of MgAl-L (003) ($2\theta=11.3$ °), after introducing Pr, the diffraction peak slightly decreases. According to the Bragg equation calculation, $2d\sin\theta=n\lambda$ [30], the crystal plane spacing d_{003} of MgAl-L is 0.79 nm, the d_{003} of Pr-0.025-L and Pr-0.05-L is 0.8 nm, and the d_{003} of Pr-0.1-L and Pr-0.2-L is 0.81 nm. From this, it can be seen that the d_{003} of hydrotalcite will increase due to the doping of Pr, and as the proportion of Pr doping increases, the d_{003} will also increases. As the atomic radius of Pr (1.83) is larger than that of Al (1.43), and as the proportion of Pr increases, it will replace more parts of Al atoms, so the layer spacing d_{003} becomes larger.

3.2 morphological analysis

The morphology of hydrotalcite and its mixed oxide is shown in Fig.2. It can be seen that MgAl-L has a typical layered structure, and the particles of hydrotalcite are relatively large (Fig.2a). The morphology of the mixed oxide formed after calcination at 500 °C transforms into smaller flakes. The ternary hydrotalcite formed by introducing Pr into MgAl-L still has the layered structure of hydrotalcite (Fig.2c). After calcination at different temperatures, its morphology underwent significant changes, transforming into small flakes. As the calcination temperature increases, the resulting flakes are also approximately regular. This is similar to the results mentioned in the literature [16].
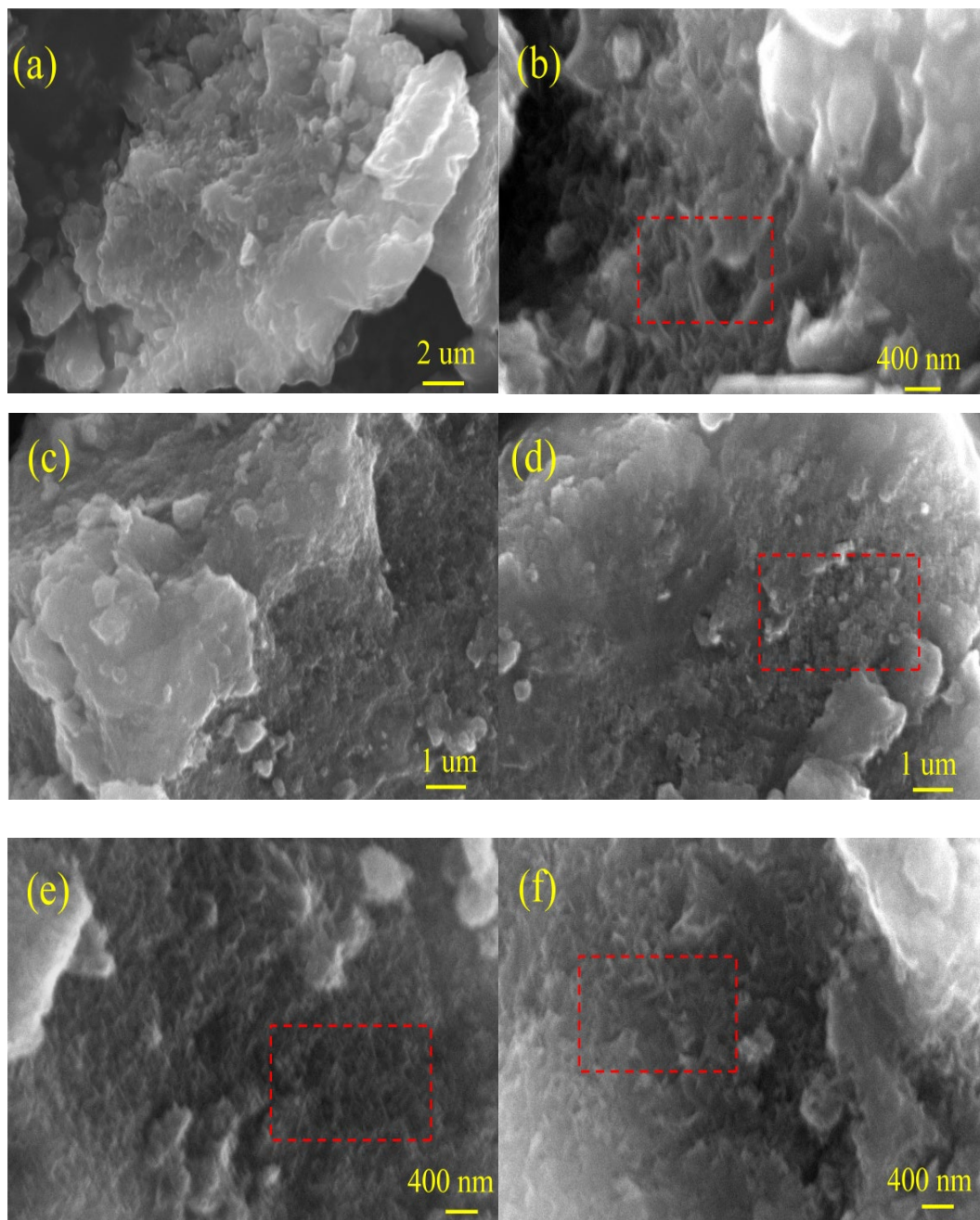
Fig. 2. SEM images of (a)MgAl-L, (b)MgAl-LDO-500, (c)Pr-0.05-L, (d)Pr-0.05-400, (e)Pr-0.05-500 and (f)Pr-0.05-600.

Comparing the morphology of hydrotalcite samples with different pr contents after calcination at 500 ℃ (Fig.3a-d), it is found that the mixed oxide exhibits small particles with a particle size of approximately 200 nm, and the Pr content has little effect on the morphology of the mixed oxide.
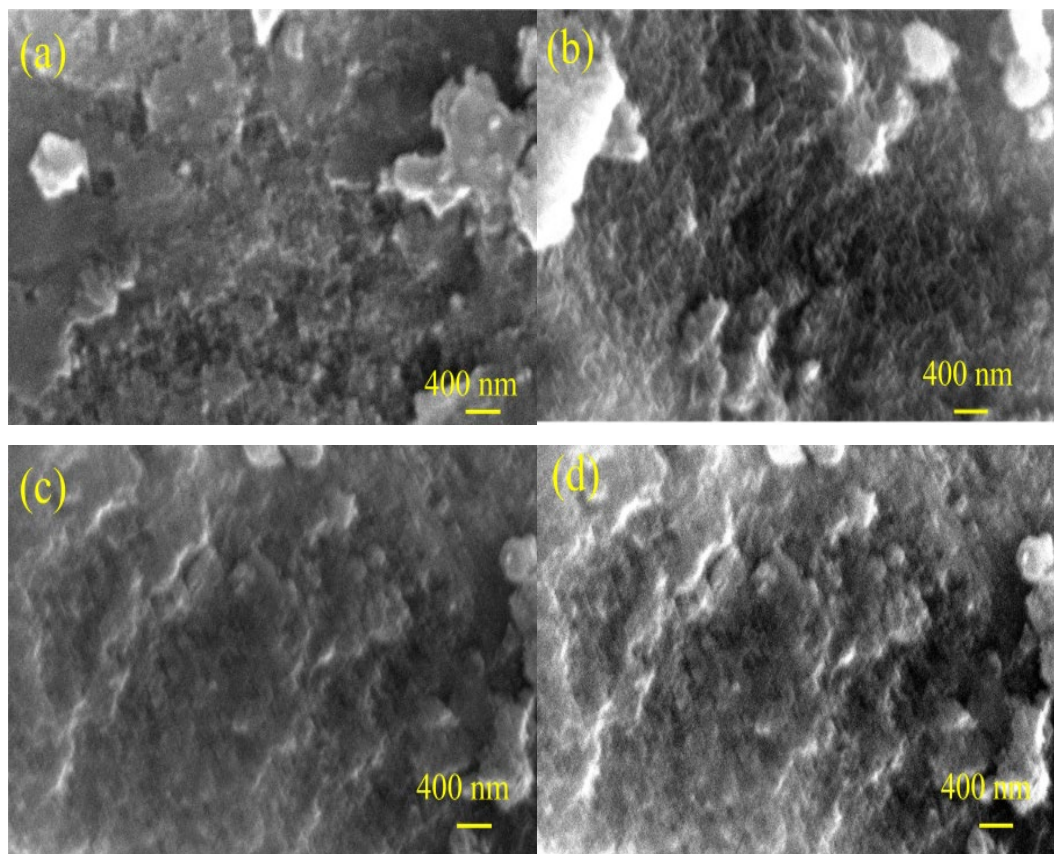
Fig. 3. SEM images of (a)Pr-0.025-500, (b)Pr-0.05-500, (c)Pr-0.1-500, and (d)Pr-0.2-500.

3.3. TG-DTA curves

Fig. 4(a) shows the TG curves of MgAl-L and Pr-*x*-L (*x*: 0.025,0.05,0.1 and 0.2). The thermal behavior of these compounds has two stages during the heating process: room temperature to 250 °C and 250~600 °C. The order in which the final quality loss rate of the test sample decreases is as follows: Pr-0.05-L＜Pr-0.1-L＜Pr-0.2-L＜Pr-0.05-L＜MgAl-L.

Fig. 4b shows that the thermal decomposition of MgAl-L and Pr-x-L involve two distinct endothermic processes. The endothermic peak (50~ 250 °C) can be attributed to the removal of water that adsorbed on the surface and interlayer of hydrotalcite. The endothermic peak within the range of 300~600 °C is attributed to the dehydration of laminated hydroxyls, the decomposition of interlayer CO_3^{2-}, and the release of CO_2 [31]. By analyzing the DTA curve, the thermal decomposition temperature of Pr-*x*-L are higher than that of MgAl-L in the second stage, indicating that the thermal stability of Pr-*x*-L is better than that of MgAl-L. The introduction of Pr improves the thermal stability of the Pr-*x*-L, and the thermal stability performance of Pr-0.05-L is best. The DTA curve further indicates that at the experimental calcination temperature of 400 to 600 °C, hydrotalcite can be transformed into mixed metal oxide.
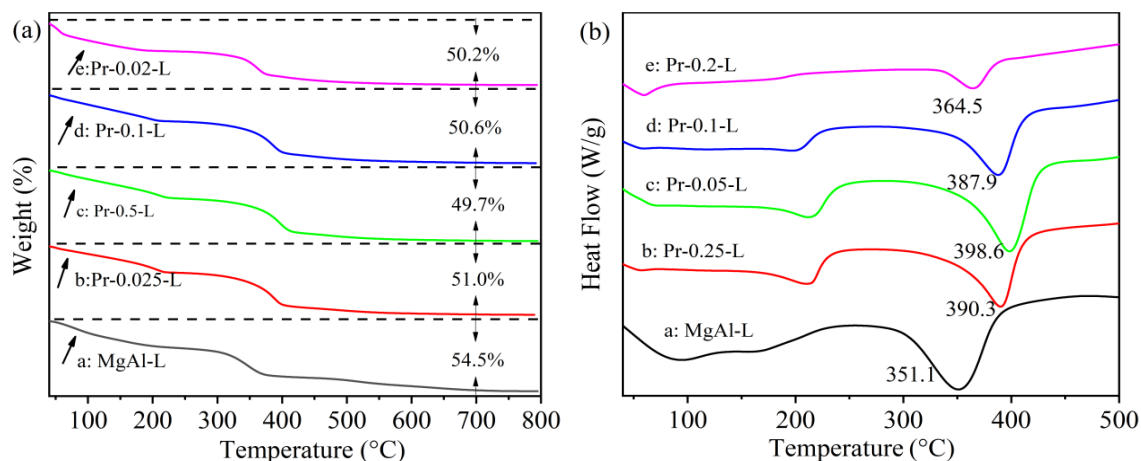
Fig. 4. TG (a) and DTA (b) curves of MgAl-L and Pr-x-L (x: 0.025, 0.05, 0.1 and 0.2).

3.4 UV–Vis DRS analysis

In Fig.5(a-i), MgAl-L, MgAl-LDO, Pr-*x*-L, and Pr-*x*-LDO all exhibit good absorption in the range of visible light. The absorption range of light by MgAl-L and MgAl-LDO is mainly concentrated in 200~400 nm. However, Pr-*x*-L and Pr-*x*-y exhibit absorption above 400 nm and have well photocatalytic activity in the visible light region, indicating an improvement in the photocatalytic ability of Pr-*x*-L and Pr-*x*-y mixed oxide [16, 17].

Fig.5(a-i) show the diffuse reflection curves of the experimental synthesized samples. Using the data obtained from the diffuse reflection test, the band gap Eg values of each sample were obtained, as shown in the table 1. The Eg value of MgAl-L is 3.53 eV, and the Eg values of the mixed oxide after calcination range from 2.73 to 2.92 eV. Comparing the Eg values in the table 1, it is found that the Eg values of Pr-*x*-L (*x*=0.025~0.2) range from 2 to 2.02 eV, which is significantly smaller than that of MgAl-L. The Eg values of the MMO are also smaller than those of the MgAl-L based mixed oxide. The temperature of calcination has little effect on the Eg value of mixed oxide, with the Eg values of mixed oxide range from 1.68 to 1.87 eV. In addition, comparing the Eg values of mixed oxide at different temperatures, it is found that Pr-0.025-L and Pr-0.05-L have the lowest Eg values after calcination at 500 ℃. However, Pr-0.1-L and Pr-0.2-L have the lowest Eg value as the calcination temperature increases. The above results indicate that the introduction of Pr enhances the photocatalytic activity of MgAl-L, and the products of hydrotalcite based mixed oxide further improve photocatalytic activity.
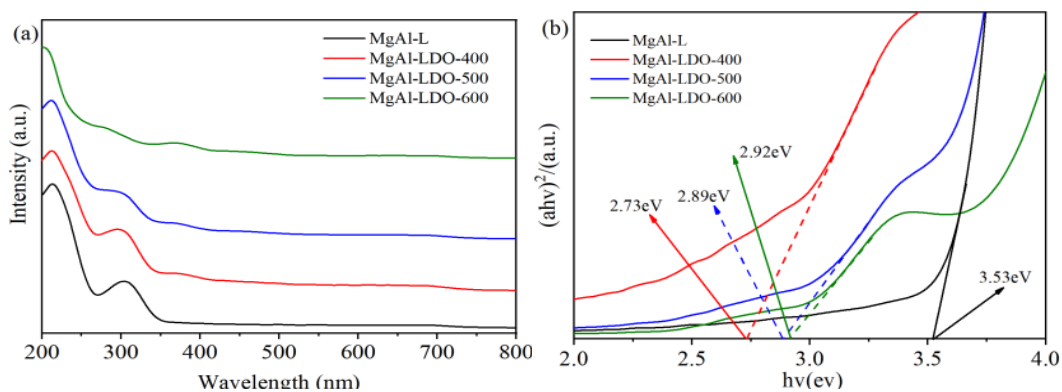

Fig. 5.1. DRS spectra of MgAl-L, Pr-x-L (x: 0.025, 0.05, 0.1 and 0.2) and mixed oxide (a, c, e, g, i), plots of the (ahv)² versus hv of MgAl-L, Pr-x-L (x: 0.025, 0.05, 0.1 and 0.2) and mixed oxide (b, d, f, h, j).

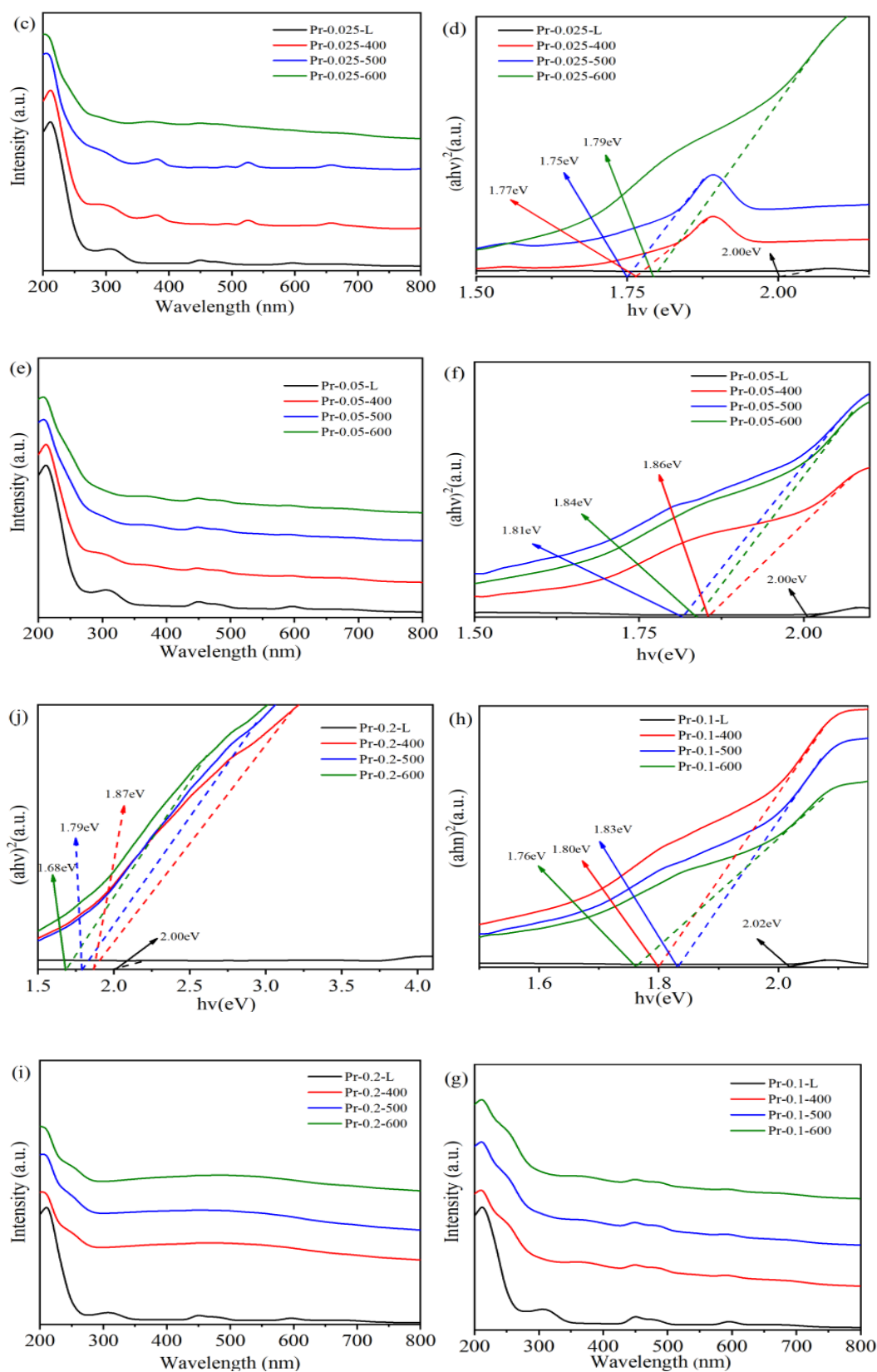*Fig. 5.2. DRS spectra of MgAl-L, Pr-x-L (x: 0.025, 0.05, 0.1 and 0.2) and mixed oxide (a, c, e, g, i), plots of the (ahv)² versus hv of MgAl-L, Pr-x-L (x: 0.025, 0.05, 0.1 and 0.2) and mixed oxide (b, d, f, h, j).*

Table 1. The band gap Eg values of samples.

Sample	Uncalcined /eV	Calcined at 400 °C/eV	Calcined at 500 °C/eV	Calcined at 600 °C/eV
MgAl-L	3.53	2.73	2.92	2.89
Pr-0.025-L	2.00	1.77	1.75	1.79
Pr-0.05-L	2.00	1.86	1.81	1.84
Pr-0.1-L	2.02	1.80	1.83	1.76

3.5. Photocatalytic degradation of MB

The photocatalytic degradation of MB by MgAl-L and their mixed oxide produced at different calcination temperatures are shown in Fig.6a.
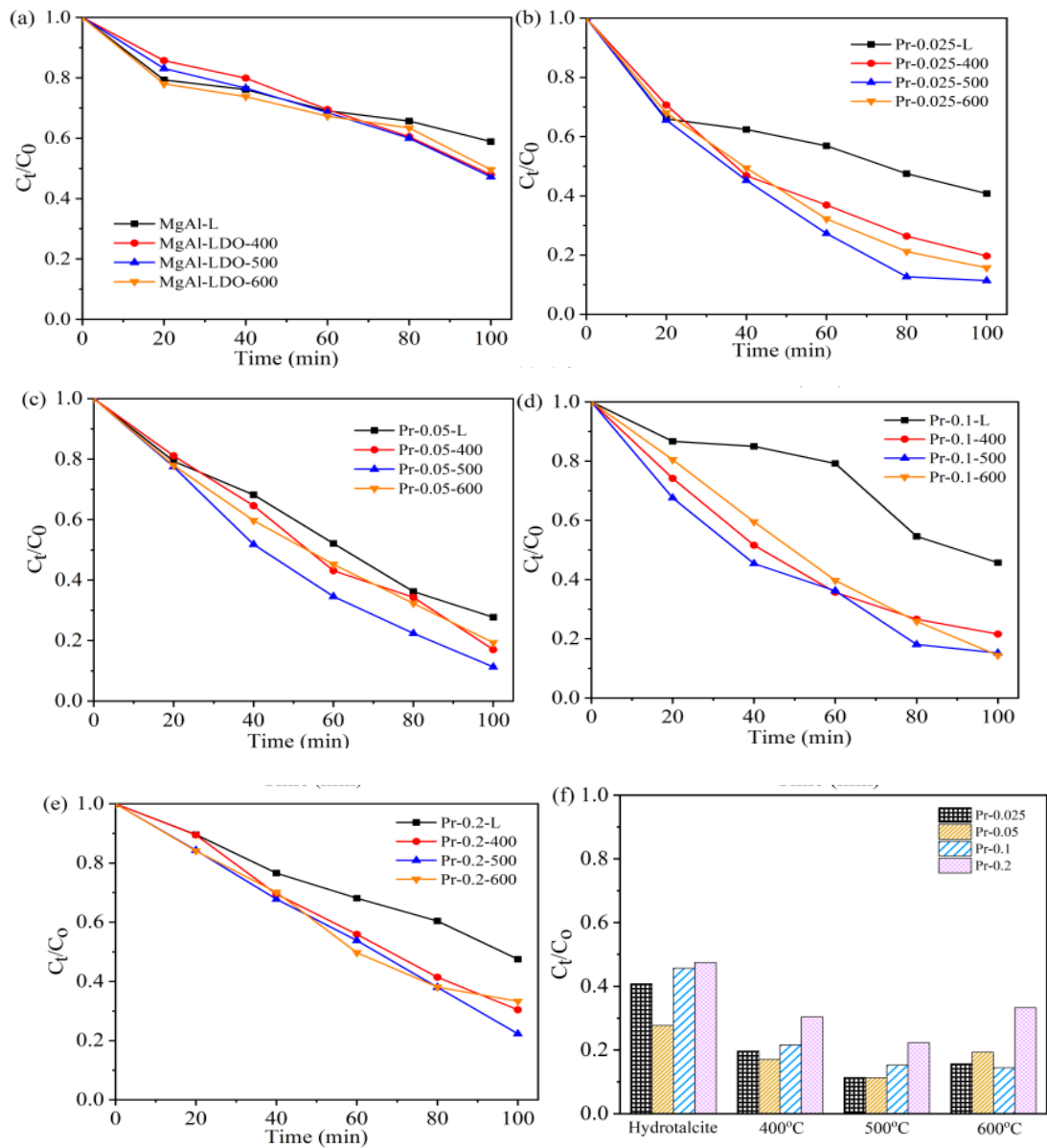

Fig. 6. Photocatalytic degradation of MB with MgAl-L, Pr-x-L and their mixed oxide.

As the illumination time prolongs, the residual rate about MB decreases gradually. In addition, after 100 min of illumination, the residual rates of MB after photocatalytic degradation with MgAl-LDHs, MgAl-LDO-400, MgAl-LDO-500, and MgAl-LDO-600 are 58.9%, 47.9%, 47.2%, and 49.6%, respectively. This indicates that both MgAl-L and their mixed oxide have photocatalytic activity. The residual rate of photocatalytic degradation of MB solution at MgAl-LDO-500 is the lowest, with a removal rate of 47.2%, indicating that MgAl-LDO-500 has the best photocatalytic effect on MB. According to Fig.6b-e, the photocatalytic performance of MgAl-L and Pr-x-L (x: 0.025, 0.05, 0.1 and 0.2), the data under 100 min of illumination were selected for comparison. It can be seen that the residual rate of MB under the catalytic degradation with MgAl-L is 58.9%, and the residual rates of MB under the catalytic degradation with Pr-0.025-L, Pr-0.05-L, Pr-0.1-L, and Pr-0.2-L are 40.8%, 27.7%, 45.7%, and 47.5%, respectively. This indicates that both MgAl-L and Pr-x-L can photocatalytic degrade MB, and Pr-x-L have slightly better photocatalytic degradation effect than MgAl-L. Meanwhile, the photocatalytic degradation of MB by Pr-0.05-L is more effective than that of Pr-0.025-L, Pr-0.1-L and Pr-0.2-L.

The photocatalytic degradation of MB by hydrotalcite and its mixed oxide with different Pr contents is also shown in Fig.6(b-e). Comparing the photocatalytic effect, it is found that both Pr-x-L and Pr-x-y can photocatalytic degrade MB, and the photocatalytic effect of mixed oxide is better than that of hydrotalcite. From Fig.6(b-e), the photocatalytic effects of Pr-0.05-L and mixed oxide at different calcination temperatures are studied. After 100 min of illumination, the residual rates of MB by Pr-0.05-L, Pr-0.05-400, Pr-0.05-500, and Pr-0.05-600 are 27.7%, 17%, 11.3%, and 19.3%, respectively. This indicates that both Pr-0.05-L and their mixed oxide have photocatalytic performance, and Pr-0.05-500 has the best photocatalytic degradation effect. At this time, the degradation rate of MB solution can reach 88.7% after 100 min of light irradiation.

In order to compare the photocatalytic degradation effect of mixed oxide more intuitively, we compared the residual rate of MB after 100 min irradiation, as shown in Fig.6f. From the column chart, it can be seen that the photocatalytic effect of mixed oxide is better than that of hydrotalcite. The photocatalytic effect of doping Pr ratios of 0.025 mol, 0.05 mol, and 0.2 mol is as follows: Pr-x-500>Pr-x-400>Pr-x-600>Pr-x-L, and the photocatalytic effect of Pr (0.1 mol) is as follows: Pr-0.1-500>Pr-0.1-600>Pr-0.1-400>Pr-0.1-L. Overall, the catalytic degradation effect of Pr mixed oxide generated by calcination at 500 °C is superior to other calcination temperatures. Under calcination at 500 °C, Pr-0.05-500 has the best catalytic degradation effect on MB, surpassing other Pr-x-L and Pr-x-y.

3.6 Photocatalytic degradation mechanism

In the presence of disodium ethylenediaminetetraacetate (EDTA), isopropanol (IPA) and p-benzoquinone (BQN), as scavengers for photo excited holes ($h+$), hydroxyl radicals ($\cdot OH$) and superoxide radicals ($\cdot O_2^-$), respectively, the reaction species were determined to further elucidate the reaction mechanism [16, 32]. In addition, the molar ratio of capturing agent to MB is controlled at 100:1. After irradiated for 100 min (Fig.7), the residual rate of MB is 45.1%, 37% and 26.7% over EDTA, BQN and IPA, respectively. Compared with the reaction conditions without a capture agent (residual rate is 11.3%), the residual rate of MB increases, indicating a decrease in the removal rate of MB, indicating that the addition of a capture agent reduces the photocatalytic effect. This is due to the addition of capture agents capturing the active species in the photocatalytic experiment, resulting in a decrease in the photocatalytic effect [16, 33]. Further analysis reveals that in the presence of EDTA, a significant decrease in MB degradation is observed, indicating that $h+$ plays a major role in the degradation of MB. In addition, adding IPA and BQN to the photocatalytic reaction system, the degradation of MB slightly decrease, indicating that $\cdot OH$ and $\cdot O_2^-$ corresponding to the capture agent are less important for the photocatalytic degradation of MB [33, 34].
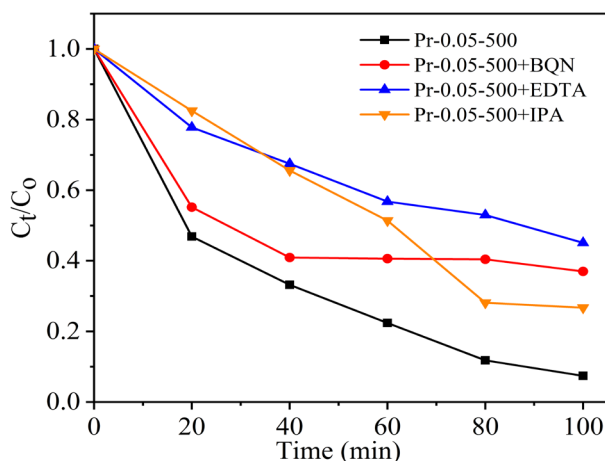
Fig. 7. Photocatalytic degradation of MB with scavengers.

Based on experimental results and combined with references [27, 28], a possible mechanism of the photocatalytic reaction of Pr-0.05-500/H_2O_2 is proposed. The photogenerated e^- and $h+$ will be generate at the interface of Pr-0.05-500 under visible light irradiation. The generated e^- and $h+$ can freely move within Pr-0.05-500. When these e^- and $h+$ move to the surface of the catalyst, e^- will interact with O_2 and H_2O_2 in solution to generate $\cdot O_2^-$ and $\cdot OH$, and $h+$ will react with H_2O_2 to generate $\cdot OH$. Finally, the generated $\cdot OH$ can promote the oxidative decomposition of MB. Furthermore, the $h+$ plays a crucial role, the $\cdot O_2^-$ and $\cdot OH$ are the less important reactive species in the photocatalytic degradation of MB by Pr-0.05-500/H_2O_2 reaction system [16].

3.7. Color difference analysis

The CIE colorimetric testing is used to further investigate the color differences of mixed oxide formed calcination of LDHs (table 2). Comparing the L^* values in the table 2, it is found that the L^* values of MgAl-L and Pr-0.05 are 93.69 and 94.57, respectively, indicating high brightness of the samples. However, after calcination, the L^* value of LDHs changes significantly. The L^* value of MgAl-LDO-400 is 90.04, with a slight decrease. But, the L^* value of MgAl-LDO-500 decreases significantly, with a L^* value of 75.1, while the L^* value of MgAl-LDO-600 increases. Comparing the a^* values, the a^* value of MgAl-L is greater than 0, implying MgAl-L has a red tone in color. However, after calcination temperature range from 400 to 600 °C, the a^* values of mixed oxide are all less than 0, indicating mixed oxide derived from MgAl-L have a green tone in color. The values of b^* of MgAl-L and its oxide derived change from negative to positive, indicating that the color changes from blue tone to yellow tone after calcination.

After calcination, the L^* value of Pr-0.05 significantly decreases, with the L^* value of Pr-0.05-500 decreasing to the lowest of 78.8. In addition, as the calcination temperature increases, the a^* value changes from negative to positive, indicating that the color of the mixed oxide tends towards the red tone. Comparing the samples of LDHs with different Pr contents calcined at 500 °C, it is found that the L^* value of the mixed oxide significantly decreases with the increase of Pr content, with the L^* value of Pr-0.1-500 being the minimum of 70.21. In addition, comparing the a^* value, it is found that except for the a* value of Pr-0.025-500, which is less than 0 and has a green tone, the other three mixed oxide containing Pr have the a^* value greater than zero and have a red tone. The b^* values of both Pr-x-L and Pr-x-y are positive, with a slightly yellow tone.

Table 2. Color difference parameters of LDHs and mixed oxide.

Sample	L*	a*	b*	Cab*	Hab*
MgAl-L	93.69	0.04	-0.11	0.12	288.54
MgAl-LDO-400	90.04	-0.44	1.59	1.65	105.39
MgAl-LDO-500	75.1	-1.51	4.95	5.18	106.99
MgAl-LDO-600	91.37	-0.98	6.22	6.3	98.97
Pr-0.05	94.57	-1.96	3.09	3.66	122.32
Pr-0.05-400	88.32	0.4	4.03	4.05	84.32
Pr-0.05-500	78.8	2.98	5.21	6	60.19
Pr-0.05-600	87.86	0.9	2.93	3.06	72.87
Pr-0.025-500	94.5	-1.07	3.4	3.57	107.46
Pr-0.05-500	78.8	2.98	5.21	6	60.19
Pr-0.1-500	70.21	4.68	3.58	5.89	37.39
Pr-0.2-500	72.83	3.75	1.44	4.02	20.99

In order to better display color differences, the color coordinates of the samples were calculated. In CIE diagram (Fig. 8), MgAl-L (point a) presents a yellow green tone, but the color display of MgAl-LDO-500 (point b) leans towards yellow tone. When a small amount of Pr is added to the composite oxide, the color of Pr-0.025-500 (point c) tends to be greenish compared to MgAl-LDO-500. As the added Pr content increases, the color of the composite oxide slightly changes (point d, point e, and point f), presenting a yellow green color tone, but the change in CIE coordinate color is very small.
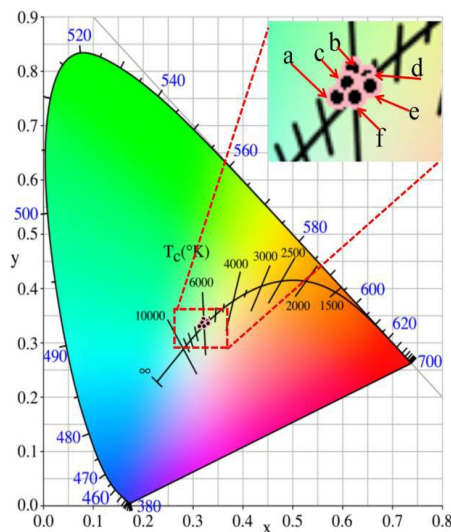

Fig. 8. Chromatic diagram of Sample. Point a: MgAl-L, point b: MgAl-LDO-500, point c: Pr-0.025-500, point d: Pr-0.05-500, point e: Pr-0.1-500, point f: Pr-0.2-500.

Comparing the colors of mixed oxide, it is found that there is a corresponding relationship between the photocatalytic performance and $L*$ value of mixed oxide based on MgAl-L and Pr-0.05. When the $L*$ value is smaller, the brightness of the mixed oxide is lower, it is easier to absorb the light source, and the photocatalytic performance is also higher. Furthermore, as the Pr content increases, the brightness of the mixed oxide also decreases, but the photocatalytic activity does not show a corresponding relationship, which may be related to the composition and structure of the calcined mixed oxide.

3.8 Optical performance

Figure 8 shows the diffuse reflectance of prepared LDHs and mixed oxide. The near-infrared reflectance (NIR) of MgAl-L is 72.05%, and after calcination, the NIR shows a significant decrease, indicating that the NIR of mixed oxide derived from MgAl-L is lower than that of MgAl-L. The NIR of Pr-0.05-L is 74.34% (Fig.8b), slightly better than that of MgAl-L, indicating that the introduction of Pr can enhance the NIR performance of LDH. In addition, the NIR of the mixed oxide generated after Pr-0.05-L calcination slightly decreases. From the spectrum, it can be seen that the decrease in reflectance is mainly concentrated at the wavelength of 750~1250 nm [35].

Comparing the NIR of mixed oxide with different Pr contents (calcined at 500 °C) (Fig.8c), it is found that the highest reflectance of Pr-0.025-500 is 75.74%, which is better than that of MgAl-LDO-500 (65.7%), indicating that the introduction of Pr can improve the NIR of mixed oxide derived from MgAl-L. The reflectivity of the other three mixed oxide Pr-x-500 (x=0.05, 0.1, 0.2) ranges from 62% to 65%. The NIR test results show that the NIR of hydrotalcite or Pr containing hydrotalcite is greatly affected by the calcination temperature and Pr content, but the NIR is greater than 50%, which is expected to be used as a near-infrared reflective material.
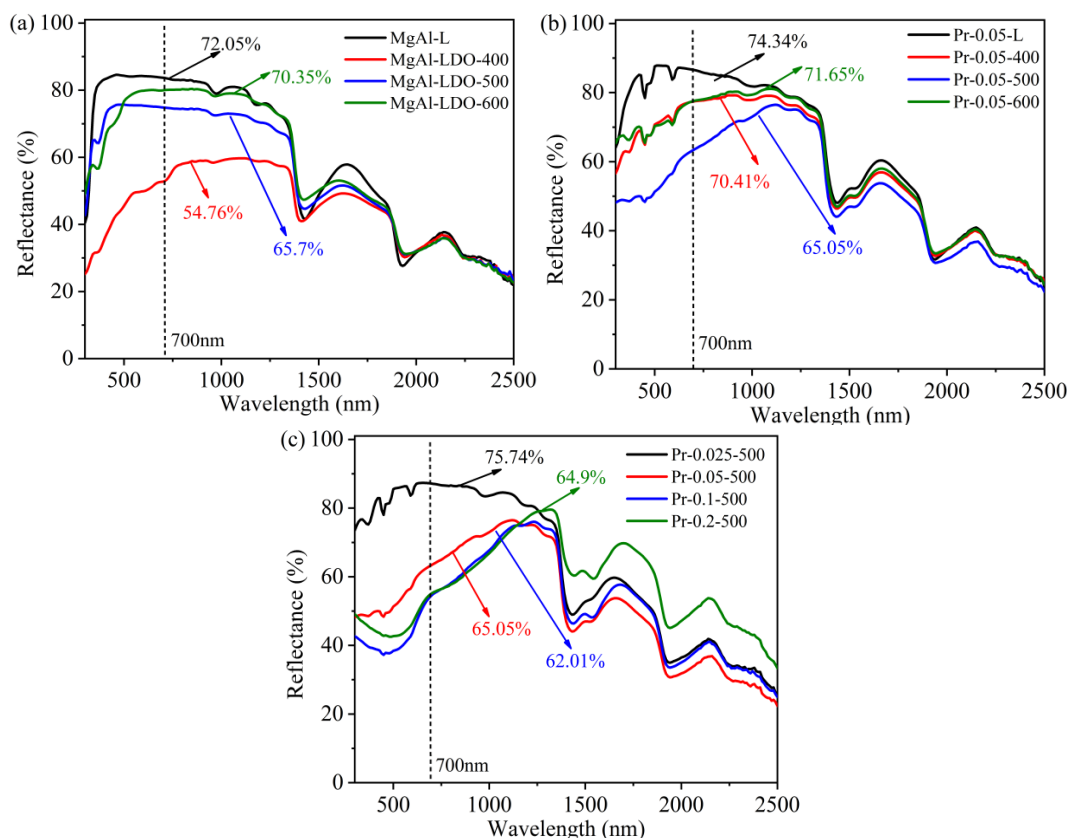

Fig. 9. Near-infrared reflectance of LDH and mixed oxide.

4. Conclusion

Different contents of Pr doped MgAlPr ternary hydrotalcite (Pr-x-L (x=0.025, 0.05, 0.1 and 0.2)) were synthesized by co-precipitation method, and Pr containing metal oxide Pr-x-y (y=400, 500 and 600) derived from Pr-x-L was prepared by high-temperature calcination. The MgAl$_2$O$_4$ is formed after calcination of MgAl-L, and the introduction of Pr slightly increases the interlayer spacing of hydrotalcite. In addition, the introduction of Pr has little effect on the morphology of hydrotalcite, but significantly improves the heat resistance of MgAl-L. In particular, the Eg value of mixed oxide containing Pr ranges from 1.68 to 1.87 eV, and Pr improves the photocatalytic activity of the mixed oxide. The experiment of visible light catalytic degradation of MB showed that the Pr-

0.05-500 had the best effect on the degradation of MB, after visible light irradiation for 100 min, the degradation rate of MB reached 87.7%. The photocatalytic degradation effect of MB with Pr containing hydrotalcite and its mixed oxide is better than that without Pr. In the reaction system of Pr-0.05-500/H_2O_2, $\bullet O_2{}^-$, $\bullet OH$, and $h+$ are all active substances in the reaction, but $h+$ played a major role. The change of Pr containing mixed oxide in CIE coordinate color is very small. There is a corresponding relationship between the photocatalytic performance and $L*$ value of mixed oxide based on MgAl-L and Pr-0.05-L. The NIR of hydrotalcite or Pr containing hydrotalcite is greatly affected by the calcination temperature and Pr content, but the NIR is greater than 50%, which is expected to be used as a near-infrared reflective material.

Acknowledgments

Declaration of Competing Interest

The authors declare that they have no known competing financial interests or personal relationships that could have appeared to influence the work reported in this paper.

Data availability

Data will be made available on request.

References

[1] S. Mallakpour, M. Hatami, C.M. Hussain, Adv. Colloid. Interfac., 283, 102216, (2020); https://doi.org/10.1016/j.cis.2020.102216

[2] C.Peng, J. Yu, Z. Zhao, J. Fu, M.Zhao, W.Wang, J.Dai, Cold. Reg. Sci. Technol., 110, 70-76, (2015); https://doi.org/10.1016/j.coldregions.2014.11.013

[3] J. Wang, B. Huang, Z. Mao, Y. Wang, Materials, 14, 994, (2021); https://doi.org/10.3390/ma14040994

[4] R. Trujillano, C. Nájera, V. Rives, Catalysts. 10, 702, (2020); https://doi.org/10.3390/catal10060702

[5] X. Tian, Z. Hao, C. Wang, J. Dong, L. Wang, L. Ma, Y. Gao, Z.G. Ha, R. Zhang, J. Colloid Interf. Sci. 645, 319, (2023); https://doi.org/10.1016/j.jcis.2023.04.151

[6] W. Long, J. Xie, X. Zhang, Y. Fang, K.H. Khayat, Cement Concrete Comp. 123, 104213, (2021); https://doi.org/10.1016/j.cemconcomp.2021.104213

[7] C. Zhou, Appl. Clay Sci., 48, (2010); https://doi.org/10.1016/j.clay.2009.12.018

[8] X. Xiang, L. Xie, Z. Li, F. Li, Chem. Eng. J., 221, 222-229, (2013); https://doi.org/10.1016/j.cej.2013.02.030

[9] H. Dib, R.E. Khawaja, G. Rochard, C. Poupin, R. Cousin, Catalysts. 10, 870, (2020); https://doi.org/10.3390/catal10080870

[10] M. Yu, L. Zhang, J. Wen, H. Zhang, F. Liu, Y. Lv, X. Zhao, J. Inorg. Organomet. P. , 32, 973-983, (2022); https://doi.org/10.1007/s10904-021-02166-z

[11] O.V. Nestroinaya, I.G. Ryl'tsova, E.A. Tarasenko, M.N. Yapryntsev, A.A. Solov'eva, O.E. Lebedeva, Petrol. Chem. 61, 388, (2021); https://doi.org/10.1134/S096554412103004X

[12] P.H. Chang , Z. Li , W.T. Jiang, Appl.Clay Sci. 190, 105563, (2020); https://doi.org/10.1016/j.clay.2020.105563

[13] T. Turk, T. Boyraz, B. Alp, Environ. Geochem. Hlth. 42, 1335, (2019); https://doi.org/10.1007/s10653-019-00420-5

[14] S. Chen, F. Yang, Z. Cao, C. Yu, H. Zhong, Colloid. Surface. A; 586, 124, (2019). https://doi.org/10.1016/j.colsurfa.2019.124140

[15] N.F. Balsamo, S.N. Mendieta, A. Vasiliev, M.E. Crivello, Adsorption; 25, 1329, (2019); https://doi.org/10.1007/s10450-019-00095-5

[16] M. Xu, M. Qian, G. Pan, Y. Guo, T. Wu, Clay Clay Miner. 67, 253, (2019); https://doi.org/10.1007/s42860-019-00023-2

[17] M. Aloui, R. Dardouri, S.B. Ghorbel, M.G. Álvarez, F. Medina, M.S. Zina, Inorg. Nano-Met. Chem. 52, 1430, (2022); https://doi.org/10.1080/24701556.2021.1956967

[18] X. Sun, L. Li, T. Hu, Q. Lian, Y. Liu, J. Hou, Y. Yu, Y. Cao, F. Ma, Colloid. Surface. A. 658, 130744, (2023); https://doi.org/10.1016/j.colsurfa.2022.130744

[19] P. Pinthong, P. Praserthdam, B. Jongsomjit, J. Oleo Sci. 68, 679, (2019); https://doi.org/10.5650/jos.ess19035

[20] M.F. De Almeida, C.R. Bellato, L.D.L. Miranda, J.L. Milagres, Ceram. Int. 43, 1843, (2016); https://doi.org/10.1016/j.ceramint.2016.10.143

[21] J. Zhang, N. Xu, Catalysts. 10, 54, (2020); https://doi.org/10.3390/catal10010054

[22] R. Levinson, H. Akbari, P. Berdahl, Sol. Energy. 84, 1717, (2010); https://doi.org/10.1016/j.solener.2010.04.018

[23] R. Levinson, H. Akbari, P. Berdahl, Sol. Energy. 84, 1745, (2010); https://doi.org/10.1016/j.solener.2010.04.017

[24] M. Xu, G. Pan, Q. Shen, Y. Guo, M. Zhou, Q. Liang, Appl. Surf. Sci., 641 158525, (2023); https://doi.org/10.1016/j.apsusc.2023.158525

[25] K. Kaneda, T. Mizugaki, Green Chem. 21, 1361, (2019); https://doi.org/10.1039/C8GC03391A

[26] S.G. Menon, H.C. Swart, J. Alloy Compd. 81, 152991, (2020); https://doi.org/10.1016/j.jallcom.2019.152991

[27] Y. Li, Y. Le, Z. Wang, Y. Hong, Q. Pu, Appl. Surf. Sci. 508, 145266, (2020); https://doi.org/10.1016/j.apsusc.2020.145266

[28] O.P. Ferreira, O.L. Alves, D.X. Gouveia, A.G.S. Filho, J.A.C.D. Paiva, J.M. Filho, J. Solid State Chem. 177, 3058, (2004); https://doi.org/10.1016/j.jssc.2004.04.030

[29] D.C. Carvalho, N.A. Ferreira, J.M. Filho, O.P. Ferreira, J.M. Soares, A.C. Oliveira, Catal.

Today. Today. 250, 155, (2015);
https://doi.org/10.1016/j.cattod.2014.08.010

[30] M. Ye, M. Li, X. Qin, M. Gao, J. Liu, Xi. Yu, Ceramics International, 49, 16, (2023);
https://doi.org/10.1016/j.ceramint.2023.05.236

[31] T. Hibino, Y. Yamashita, K. Kosuge, A. Tsunashima, Clay Clay Miner. 43, 427, (1995);
https://doi.org/10.1346/CCMN.1995.0430405

[32] T. Yan, H. Zhu, R. Li, Z. Li, J. Liu, G. Wang, Electrochim. Acta. 111, 71, (2013);
https://doi.org/10.1016/j.electacta.2013.07.215

[33] M. Xu, G. Pan, Y. Meng, Y. Guo, T. Wu, H Chen, Appl. Clay Sci. 170, 46, (2019);
https://doi.org/10.1016/j.clay.2019.01.011

[34] R. Thambidurai , G. Gobi , R. Uthrakumar, C. Inmozhi , K. Kaviyarasu, Dig. J. Nanomater. Bios. 869, 18, (2023);
https://doi.org/10.15251/DJNB.2023.183.869

[35] Q. Xiang, J. Yu, P.K. Wong, J. Colloid Interf. Sci. 357, 163, (2011);
https://doi.org/10.1016/j.jcis.2011.01.093